PLOS NEGLECTED TROPICAL DISEASES

RESEARCH ARTICLE

Simulation models of dengue transmission in Funchal, Madeira Island: Influence of seasonality

Donald Salami[1]*, César Capinha[2], Carla Alexandra Sousa[1]*, Maria do Rosário Oliveira Martins[1], Cynthia Lord[3]*

1 Global Health and Tropical Medicine, Instituto de Higiene e Medicina Tropical, Universidade Nova de Lisboa, Lisbon, Portugal, **2** Centro de Estudos Geográficos, Instituto de Geografia e Ordenamento do Território, Universidade de Lisboa, Lisbon, Portugal, **3** Florida Medical Entomology Laboratory, Institute of Food and Agricultural Sciences, University of Florida, Vero Beach, Florida, United States of America

* donald.salami@gmail.com (DS); casousa@ihmt.unl.pt (CS); clord@ufl.edu (CL)

Citation: Salami D, Capinha C, Sousa CA, Martins MdRO, Lord C (2020) Simulation models of dengue transmission in Funchal, Madeira Island: Influence of seasonality. PLoS Negl Trop Dis 14(10): e0008679. https://doi.org/10.1371/journal.pntd.0008679

Editor: Christopher M. Barker, University of California, Davis, UNITED STATES

Received: October 28, 2019

Accepted: August 4, 2020

Published: October 5, 2020

Data Availability Statement: All relevant data are within the manuscript and its Supporting Information files.

Funding: DS has a PhD grant from the Fundação para a Ciência e a Tecnologia (FCT), Portugal (https://www.fct.pt/), grant number: PD/BD/128084/2016 This work was also partially funded by FCT grants awarded to CS, grants number: Project Warden - PTDC/SAU-PUB/30089/2017 and GHTM–UID/Multi/04413/2020. CC acknowledges support from FCT, grants number: CEECIND/

Abstract

The recent emergence and established presence of *Aedes aegypti* in the Autonomous Region of Madeira, Portugal, was responsible for the first autochthonous outbreak of dengue in Europe. The island has not reported any dengue cases since the outbreak in 2012. However, there is a high risk that an introduction of the virus would result in another autochthonous outbreak given the presence of the vector and permissive environmental conditions. Understanding the dynamics of a potential epidemic is critical for targeted local control strategies.

Here, we adopt a deterministic model for the transmission of dengue in *Aedes aegypti* mosquitoes. The model integrates empirical and mechanistic parameters for virus transmission, under seasonally varying temperatures for Funchal, Madeira Island. We examine the epidemic dynamics as triggered by the arrival date of an infectious individual; the influence of seasonal temperature mean and variation on the epidemic dynamics; and performed a sensitivity analysis on the following quantities of interest: the epidemic peak size, time to peak, and the final epidemic size.

Our results demonstrate the potential for summer and autumn season transmission of dengue, with the arrival date significantly affecting the distribution of the timing and peak size of the epidemic. Late-summer arrivals were more likely to produce large epidemics within a short peak time. Epidemics within this favorable period had an average of 11% of the susceptible population infected at the peak, at an average peak time of 95 days. We also demonstrated that seasonal temperature variation dramatically affects the epidemic dynamics, with warmer starting temperatures producing large epidemics with a short peak time and vice versa. Overall, our quantities of interest were most sensitive to variance in the date of arrival, seasonal temperature, transmission rates, mortality rate, and the mosquito population; the magnitude of sensitivity differs across quantities.

Our model could serve as a useful guide in the development of effective local control and mitigation strategies for dengue fever in Madeira Island.

02037/2017, UIDB/00295/2020 and UIDP/00295/2020. The funders had no role in study design, data collection and analysis, decision to publish, or preparation of the manuscript.

Competing interests: The authors have declared that no competing interests exist.

Author summary

The presence of *Aedes aegypti* mosquitoes in Madeira Island had recently caused the first local outbreak of dengue in Europe. The island is at risk of another local transmission if triggered by the introduction of the dengue virus by an infected person. Using a mathematical model for the transmission of dengue, we examine the dynamics of a potential epidemic triggered by the arrival of an infected person on the island. We also examine the impact of seasonal temperature variation on the epidemic dynamics. Our results show the potential for summer and autumn season transmission of dengue on the island, and that the arrival date of an infectious person affects the distribution of the timing and peak size of the epidemic. Late summer arrivals were more likely to produce a rapid epidemic. We also show that seasonal temperature variation dramatically affects the epidemic dynamics. With warmer starting temperatures, epidemics peak faster, producing a large final epidemic size. Our model could be useful to estimate the risk of an epidemic outbreak and as a guide for local control and mitigation strategies for dengue on the island.

Introduction

Dengue is notably the most important mosquito-borne viral disease, with approximately half the world's population at risk of infection [1]. This arboviral disease, caused by a virus of the Flaviviridae family, has gained renewed global attention due to its wide geographical spread and increased burden in recent years. The spread of the disease is in concordance with the geographical expansion of its primary vector (i.e. *Aedes aegypti*), characterized by the presence of a suitable climate and increase in global trade and travel [2, 3].

A paradigmatic example of the recent spread of dengue and its epidemic potential was demonstrated in Madeira Island, an autonomous region of Portugal (S1 Fig), with an estimated population size of 270,000. *Aedes aegypti* was first detected in Funchal, the capital city of Madeira Island, in 2005 and by October 2012 the island reported its first autochthonous case of Dengue serotype 1 (DENV 1) [4]. The importance of this epidemic is demonstrated by three main reasons: (1) It was the first sustained autochthonous transmission of dengue in the European Union since the 1920s [5]; (2) its size, with 1080 confirmed cases (of the 2168 probable cases reported) and 78 cases reported in 13 other European countries in travelers returning from Madeira [6]; and (3) the rapid time course of the epidemic, the epidemic peaked within a month after the official report of the first case in October [7] with a rapid decline thereafter with no cases recorded after 3 March 2013.

To understand the complexities of this outbreak, Lourenco and Recker [8] developed an ento-epidemiological mathematical model to explore the ecological conditions and transmission dynamics. Their findings suggest the virus was introduced over a month before cases were reported (in August). In their model, asymptomatic circulation occurred before the two initial autochthonous cases were reported in October, maintaining the virus in the population. Furthermore, their findings indicate that the transmission dynamics and eventual epidemic burnout was driven predominantly by the influence of temperature on the life-history traits of the mosquitoes (incubation period, mosquito mortality and aquatic developmental rates). The seasonal drop in autumn temperatures led to a reduction of the vectorial capacity and effectively stopped the virus propagation.

Their findings are consistent with previous experimental work addressing the strong influence of temperature on the life-history traits of the mosquitoes and arbovirus transmissions [9–12]. Likewise, many existing mechanistic transmission models have integrated the effects of

temperature on mosquito traits to understand how it influences the probability and magnitude of dengue transmissions [13–17]. Other recent work examined the influence of seasonal variation in temperature on the epidemic magnitude and duration [18, 19]. These models emphasize the strong, nonlinear (often unimodal) influence of temperature and seasonality on dengue transmission and epidemic dynamics.

Expanding on previous work, we here explore the impact of seasonal temperature variations on the potential epidemic dynamics on Madeira Island. It is imperative to explore the influence of seasonality, as Madeira Island presents with a range of contrasting bioclimates because of its heterogeneous landscape and strong influence from the Gulf Stream and Canary current [20]. The southern coastal regions of the island (including Funchal), at low altitudes, have higher annual temperatures in comparison to the northern coastal regions or inland regions with higher altitudes and lower annual temperatures [20, 21]. Although the island has not reported any dengue cases since the outbreak in 2012, new introductions would likely result in local transmission given the presence of the vector and permissive environmental conditions. A recent vector competence study with *Aedes aegypti* from Madeira reported virus transmission potential (virus in saliva) from 2 Madeira populations, although the proportions transmitting was low (transmission rate of 18%, 14 days post-infection) [22]. This demonstrates the potential risk of local transmission of a different serotype of dengue, if introduced on the island. With an increase in co-circulation of all dengue serotypes (DENV 1–4) worldwide [23, 24], and Madeira's increasing lure as a popular year-round travel destination, a potential introduction is likely [25].

We incorporate a standard deterministic SEI-SEIR transmission model parameterized from existing literature and available field data. The main goals of this model are: (1) to examine the epidemic dynamics in Funchal, Madeira as triggered by the arrival of an infectious individual at different time points during the year; and (2) to examine the influence of seasonal temperature mean and variation on epidemic dynamics. To do this, we employed a different modeling framework from that of [8], in that our model explicitly accounts for seasonality and temperature dependence in the transmission dynamics. Likewise, we explore epidemiologically relevant outcomes of epidemic size, peak incidence, and time to peak, rather than basic reproduction number or vectorial capacity, which are more complex measures of epidemic dynamics.

Methods

Model framework

We adopt a deterministic compartmental vector-host transmission model exploring chikungunya virus invasion in Florida, United States with *Aedes aegypti* and *Aedes albopictus* mosquitoes, from [26]. This was adapted into a standard SEI-SEIR transmission model with one vector, similar to others used in modeling dengue transmission (e.g. in [27–30]).

The SEI component of our model describes the vector population, represented as susceptible (S_v), exposed (E_v), and infectious (I_v). Our models explicitly consider a single vector and a single life stage, i.e. adult females of *Aedes aegypti*. Mosquitoes enter the susceptible class through a recruitment term, based on observed seasonality patterns from field data in Funchal [31]. The recruitment term does not explicitly model the aquatic (eggs, larvae, and pupae) stage of mosquitoes and is not linked to the current population size, but explicitly includes seasonality in recruitment to the adult female population. A susceptible mosquito moves into the exposed class (E_v), after biting an infectious human and becoming infected with the dengue virus. After a temperature-dependent extrinsic incubation period, surviving mosquitoes get transferred to the infectious class (I_v). They remain in the infectious class until death, due to

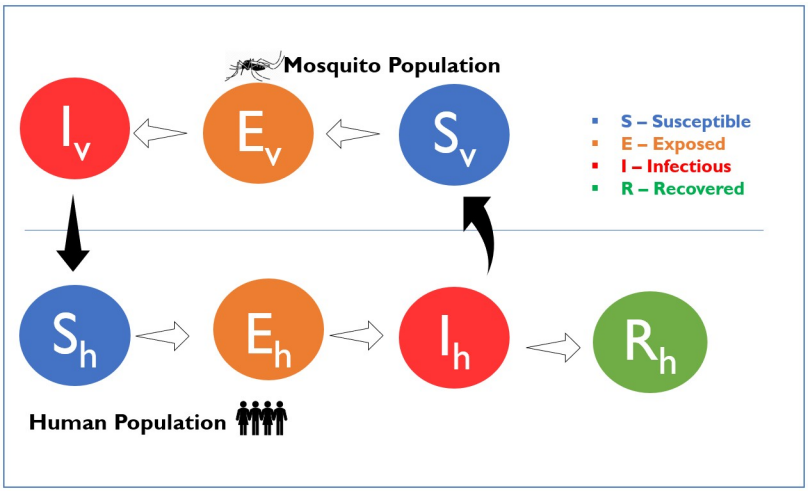

Fig 1. Schematic representation of the model. S_v, E_v, and I_v represent the susceptible, exposed, and infectious compartments of the mosquito population. S_h, E_h, I_h, and R_h represent the susceptible, exposed, infectious, and recovered compartments of the human population, respectively. The outline arrows are the transition from one compartment to the next, and the black filled arrows are the direction of transmission.

https://doi.org/10.1371/journal.pntd.0008679.g001

the assumption of the absence of immune response. Mosquitoes leave the system through a temperature-dependent mortality function. We assume the virus infection does not affect the lifespan of the mosquitoes and that there is no significant vertical transmission.

The SEIR component of our model describes the human population represented as susceptible (S_h), exposed (infected but not infectious) (E_h), infectious (I_h), and recovered (immune) (R_h). Our model assumes the human population (N_h) to be constant, not subject to demography as we considered a single outbreak with a duration in the order of a year. A susceptible individual enters the exposed class (E_h) after being successfully infected, by an infectious mosquito bite. We do not explicitly account for repeated biting, interrupted feeds, or alternative host preferences. We also assume that not every infectious bite leads to successful human infection. Once a human individual is exposed, they enter an intrinsic incubation period, until they become infectious. They then move to the infectious class (I_h) and can transmit the virus back to a susceptible mosquito. We assumed a single infectious class and did not further discriminate between the symptomatic or asymptomatic individuals as previous evidence demonstrates that asymptomatic individuals can transmit the virus [32]. We assume that humans stay infectious for a period after which they recover. Once a human individual enters the recovered/immune class (R_h), we assume a lifelong immunity, as multiple co-circulating serotypes of dengue virus were not considered. A resulting schematic representation of the model is shown in Fig 1.

Model equations

Our model is defined by the following ordinary differential equations:

$$\frac{dS_v}{dt} = \rho - \frac{a\,\beta_{h\to v}}{N_h} I_h S_v - \mu_v S_v \tag{1}$$

$$\frac{dE_v}{dt} = \frac{a\,\beta_{h\to v}}{N_h} I_h S_v - \gamma_v E_v - \mu_v E_v \tag{2}$$

$$\frac{dI_v}{dt} = \gamma_v E_v - \mu_v I_v \quad (3)$$

$$N_v = S_v + E_v + I_v \quad (4)$$

$$\frac{dS_h}{dt} = -\frac{a\,\beta_{v\to h}}{N_h} S_h I_v \quad (5)$$

$$\frac{dE_h}{dt} = \frac{a\,\beta_{v\to h}}{N_h} S_h I_v - \gamma_h E_h \quad (6)$$

$$\frac{dI_h}{dt} = \gamma_h E_h - \eta_h I_h \quad (7)$$

$$\frac{dR_h}{dt} = \eta_h I_h \quad (8)$$

$$N_h = S_h + E_h + I_h + R_h \quad (9)$$

Here, the coefficient ρ is the mosquito recruitment term (expanded below); a is the biting rate; $\beta_{h\to v}$ and $\beta_{v\to h}$ are the human-to-mosquito and mosquito-to-human transmission rates, respectively; $1/\gamma_h$ and $1/\eta_h$ represent the intrinsic incubation and human infectivity periods; $1/\gamma_v$ and μ_v represent the extrinsic incubation period and mortality rate for mosquitoes. The biting rate, EIP and mortality rates are temperature-dependent, detailed below. The state variables and parameters used for our model are displayed in Tables 1 and 2, respectively. Preliminary exploration of parameter values was performed to determine their permissibility for transmission and to define model starting conditions (see S1 File).

Mosquito recruitment. The coefficient (ρ) in Eq (1) above is the daily recruitment term of susceptible mosquitoes. The total number of female mosquitoes recruited into the population over the year is divided into two main phases: baseline, year-round recruitment, and a unimodal peak season recruitment. This is based on the seasonal pattern of mosquitoes on the island observed from the *Aedes aegypti* mosquito entomological surveillance by the Institute of health administration, IP-RAM, and the Funchal natural history museum [31, 47]. Weekly mosquito trap data is geo-processed and spatial analyzed to identify areas with mosquito

Table 1. State variables for the model.

Variables	Description
S_v	Number of susceptible mosquitoes
E_v	Number of exposed mosquitoes
I_v	Number of infectious mosquitoes
N_v	Total mosquito population size
S_h	Number of susceptible humans
E_h	Number of exposed humans
I_h	Number of infectious humans
R_h	Number of recovered humans
N_h	Total human population size

https://doi.org/10.1371/journal.pntd.0008679.t001

Table 2. Definitions and ranges of the model's parameters.

Parameter	Description	Default Value	Range	Reference
r_δ	Number of mosquitoes per host in the unimodal peak phase	2	2–6	[8, 33, 34]
p_{base}	Proportion of mosquitoes in baseline recruitment	0.05		[8, 35]
iv	The interval between baseline pulses (days)[1]	5	2–7	[35]
q	Timing of unimodal peak (days)[1]	220	209–230	[35]
σ	The variance of the unimodal peak (days)[1]	29		[35]
R_{tot}	Total mosquito recruitment (population size)[2]			Calculated based on default value and range for r_δ above. Used in the sensitivity analysis.
a	Mosquito biting rate[3]	$0.0043T + 0.0943$		[15, 36]
$\beta_{h\rightarrow v}$	Rate of transmission from human to mosquito	0.33	0.1–0.75	[28, 33, 37]
$\beta_{v\rightarrow h}$	Rate of transmission from mosquito to human	0.33	0.1–0.75	[28, 33, 37]
μ_v	Mortality rate of mosquitoes under optimal temperatures [4]	0.04	0.02–0.06	[13, 17]
μ_{vs}	The slope of mortality function	0.05		[13, 26]
γ_v	Virus extrinsic incubation rate (at 22.5˚C)	0.04	0.04–0.07	[17, 38]
γ_{vs}	Slope of extrinsic incubation function	0.008		[38]
$1/\gamma_h$	Intrinsic incubation period (days)	6		[39, 40]
$1/\eta_h$	Human infectious period (days)	4		[8, 41–43]
N_h	The population size of humans (constant)	30000		[44]
t_{crit}	Date of arrival of infectious human (days)[5]	181	1–365	
T_{mean}	Mean annual temperature (˚C)	20	15–30	[45, 46]
T_{range}	Temperature range (˚C)[6]	5	0–15	[45, 46]

[1] Default value and range are estimates to reflect the observed seasonal activity, not an explicit fit to the island's entomological data;

[2] See Eq 15, also note this parameter was used in the sensitivity analysis to allow estimation of the relative importance of the total recruitment;

[3] Optimal temperature for biting rate: $(21^\circ C > T < 32^\circ C)$;

[4] Mosquitoes optimal survival range: $(15^\circ C > T < 30^\circ C)$;

[5] Where $t_{crit} = 1$, calendar date is February 15; hence t_{crit} of 181 is August 15; while 365 is February 14 (i.e. a complete annual period).

[6] Temperature range is given by $(T_{max} - T_{min})$.

https://doi.org/10.1371/journal.pntd.0008679.t002

activity based on the presence/absence of eggs, the number of eggs, and adult mosquitoes captured [31].

Visual inspection of the entomological data for the years 2012–2019 (weekly time-series graphs of the cumulative number of eggs and adult mosquitoes, see S2–S5 Figs) [35] demonstrate a unimodal seasonal pattern for mosquito activity during the entomological season. The unimodal peak starts around June through to early December, with other months of the year (i.e. January to May) having little to no activity. Using a Gaussian curve, we estimated the timeline for our unimodal peak recruitment to reflect this seasonal pattern as best possible.

Actual quantifications of mosquito population density remain a grey area. However, the majority of dengue models [8, 28, 33, 34, 48] have adopted the use of a mosquito-to-human ratio of 2:1. We adopted this framework for setting the estimated number of mosquitoes recruited during the unimodal peak season (r_δ). From the derived number of mosquitoes recruited during the peak season, we assumed an additional 5% to be added in the baseline, year-round recruitment (R_{base}). The recruitment of susceptible mosquitoes is specified by the

following equations:

$$\rho(t) = \rho_b\,(t) + R_{peak}\delta(t) \tag{10}$$

Where,

$$\delta\,(t) = \frac{1}{2\pi\sigma_k}\; exp\left(\frac{1(q_k - t)^2}{2\sigma_k^2}\right) \tag{11}$$

$$\rho_b(t) = \frac{R_{base}}{iv} \tag{12}$$

$$R_{peak} = r_\delta N_h \tag{13}$$

$$R_{base} = R_{peak} p_{base} \tag{14}$$

$$R_{tot} = R_{peak} + R_{base} \tag{15}$$

Here, $\rho(t)$ represents the number of adult female mosquitoes recruited per time step; $\delta(t)$ is a Gaussian distribution for the number of mosquitoes added to the population daily, during the unimodal peak season; $\rho_b(t)$ is the number of mosquitoes added to the population at intervals (iv) during the all-year-round recruitment. R_{peak} is the total number of mosquitoes recruited during the unimodal peak season; R_{base} is the total number of mosquitoes recruited during the baseline, year-round recruitment; R_{tot} is the total number of mosquitoes recruited into the population over the year.

Seasonal forcing. To introduce seasonality in our model, we allowed the temperature to vary over time by sinusoidally forcing [49]. The daily mean temperature was modeled as a cosine curve with a period of 365 days as specified below:

$$T\,(t) = \frac{T_{max} - T_{min}}{2} * \left(-\cos\left(\frac{2\pi(t-\omega)}{365}\right)\right) + T_{mean} \tag{16}$$

Here, T is temperature in Celsius; T_{max}, T_{mean} and T_{max} are the average daily maximum, mean, and minimum temperatures over the year, (t) is time measured in days, and (ω) is the phase shift to align the cosine function with the seasonal factors in Funchal. For our temperature model calibration, we extracted a 10 year (2008–2018) historical daily from Weather Underground [45]. We then calculated the 10-year historical average of the mean, minimum, and maximum for each day of the year (excluding February 29), before estimating temperature seasonality. This provided a range of the average daily temperature over a calendar year for the period. Utilizing the mean, minimum, and maximum annual average temperature, we set estimates for our seasonality parameters. To fit the sinusoidal model, we considered the occurrence of the coldest and hottest day across the years, to determine a good starting point. The occurrence of the coldest day had fewer fluctuations mostly occurring on February 15; hence we set our start point and phase shift to this day, reflecting the long-term average conditions in Funchal, Madeira (T_{max} = 22˚ C, T_{mean} = 20˚C, T_{min} = 17˚C). S6 Fig shows a fit of the sinusoidal curve to the historical temperature seasonality.

Temperature-dependent parameters. The biting rate (a) of the adult female mosquitoes is modeled to be temperature dependent as previously estimated by [15] and [36]. The biting rate increases linearly with temperature as specified by a linear equation for an optimal temperature range of $21^\circ C < T > 32^\circ C$ and a defined temperature threshold (i.e. if $T \leq 12.4$ *or*

$T \geq 37^{\circ}C$, then $a = 0$). The extrinsic incubation period (γ_v) is modeled to be temperature-dependent, modified from [50]. Using a linear temperature function, specified by a slope (γ_{vs}), the rate near the midpoint of the plausible temperatures range for vectorial capacity (set at 22.5˚C), and a defined lower temperature threshold (i.e. if $T \leq 10^{\circ}C$ then $\gamma_v = 0$). Mortality rate (μ_v) for mosquitoes were modeled as a function of temperature using a mechanistic thermal response curve as described in [13]. They fitted their data as a complex polynomial resulting in a basin-shaped curve, with optimal temperature for mosquito's survival set at a range of $15^{\circ}C > T < 30^{\circ}C$. Based on preliminary exploration of changes to the mortality function, we modified the fitted polynomial to a piecewise linear curve with fixed, minimal mortality in the same temperature range. Mortality rate then increases quickly and linearly at temperatures outside this lower and upper bound, as specified by the function slope (μ_{vs}).

Quantities of interest (QOI)

We simulated the model under default starting conditions (see S1 File) and given that a simulation evolves into an epidemic (defined as ($I_h > 2$), after the virus introduction), we analyze for the following quantities of interest (QOI): the epidemic peak size (maximum human infected ($maxI_h$) at any given point during the simulation); time to peak infection in humans (time from introduction to $maxI_h$, as $tmaxI_h$); the final epidemic size, which represents a measure of epidemic suitability (cumulative proportion of humans infected, $cumI_h/N_h$, at the final time step).

Initial introduction and epidemic dynamics

Firstly, we examine the variability in epidemic dynamics, as a function of arrival dates of an infectious human in a susceptible population. To do this, we ran simulations for introductions on all 365 calendar days of the year, with all other parameters fixed at their default values (Table 2) and default starting conditions (S1 File). Each simulation was started on February 15 (the phase shift in the annual cycle) and ran for 2 years.

Seasonal variance and epidemic dynamics

Next, we examine the epidemic dynamics as a function of seasonal temperature variation. Utilizing the same compartmental framework with default starting conditions and parameter values, we ran sets of simulations under two different temperature regimes [18]. First, we simulated a set of temperature regimes as observed in the historical decadal data for Funchal, Madeira. The mean temperature varied from 19.0 ˚C to 21.0 ˚C in increments of 0.2 ˚C, while the temperature range (i.e. $T_{max} - T_{min}$) varied from 4.0 ˚C to 6.0 ˚C, in the same increments of 0.2 ˚C, resulting in 121 simulation runs. The variability in epidemic dynamics is then examined as a function of starting temperature. Starting temperature is defined as the temperature on the day of introduction of the virus (t_{crit}), as derived from the temperature curves.

Thereafter, we simulate a wider set of temperature regimes to examine plausible future forcing scenarios based on near-term projections of seasonal temperature changes in the region of Madeira Island. Near term projection refers to projected annual mean temperature changes for the period 2016–2035 relative to a reference period 1986–2005 [46, 51]. Mean temperature was varied between 15.0 ˚C to 30.0 ˚C in increments of 0.2 ˚C, while range varied from 0.0 ˚C to 15.0 ˚C in increments of 0.2 ˚C (i.e. a total of 5776 simulation runs). It is worth noting that most of the temperatures in this regime are outside projected changes for the island's region, and very unlikely to occur in Funchal. However, by simulating a wider set of temperature regimes, we can characterize uncertainties and probable outcomes of a local epidemic across other regions on the island. This also allows us to simulate similar extreme temperature

conditions already recorded on the Funchal in recent times (for example, high temperatures of 37.8˚C on August 5, 2016, and 26.5 ˚C on December 5, 2018 [52, 53]).

Model sensitivity analysis

To characterize the model parameters exerting the most influence on our quantities of interest, we performed a variance-based global sensitivity analysis, using a combination of Latin hypercube sampling (LHS) and a multi-model inference on regression-based models (See S2 File for details). The sensitivity analysis considered the main effects and pairwise (first-order) interactions of input parameters on our quantities of interest. LHS sampling was programmed in MATLAB [54], while the multi-model inference analysis was done using the *glmulti* R package [55, 56].

Results

Initial introduction and epidemic dynamics

We examined the timing and size of the epidemic peak as a function of different arrival dates of an infectious human into the susceptible population. An epidemic outbreak occurred only for simulated arrival dates in July to November; with the first epidemic occurring on July 14. Most simulations responded unimodally with peaks occurring few weeks after the arrival of an infectious human, this was typical for summer and early autumn arrivals (i.e. July to September) (Fig 2A and 2B). However, some simulations responded bimodally, i.e. an initial small outbreak, then a prolonged low-level transmission until another outbreak occurs (Fig 2C and 2D). This prolonged transmission was typical for arrival dates in mid to late autumn season (i.e. arrival dates in October and November).

We examine this behavior further by comparing the disease progression in the human population with that of the mosquito population (Fig 2D). Simulations with an arrival date of the infectious human in October and November had a lower chance to evolve into a unimodal outbreak, because of the depletion of the mosquito population. Following the initial outbreak, a low transmission is maintained until the next seasonal peak recruitment of the mosquitoes before another outbreak. This suggests that the virus can remain viable within the population at low rates, until the next favorable season for transmission. This also means the dynamics of the epidemic is also modulated by the temporal dynamics of the mosquito population, however, this is not the focus of our analysis.

Fig 3 shows our QOI, for all simulation dates resulting in an epidemic. Epidemic peak size was bimodally distributed as a function of date of arrival, with a dip in early October. In contrast epidemic peak time monotonically decreases as a function of the date of arrival, until mid-September, and reverses to an increase with a steep spike in early October. In part, these discontinuities are reflections of scoring each run for a single peak and corresponds to the model behavior shifts from the classical rapid unimodal epidemic, to the bimodal and prolonged epidemic. Arrival dates in the summer season produced epidemics with a much faster peak time, while arrivals in autumn had a longer transmission period.

Overall, the shifts in epidemic dynamics are driven by the seasonal change (summer and autumn seasons) and its effect on transmission dynamics. The shortest epidemic peak time simulated was 93 days, with 11.4% of the susceptible population infected, with an arrival date of August 29 and a starting temperature of 22.4˚C (Fig 2A). In contrast, the longest epidemic peak time simulated was 411 days, with 3.4% of the susceptible population infected, with an arrival date of October 7 and a starting temperature of 21˚C (Fig 2C). The final epidemic sizes were 99.99% and 99.80% of the human population infected, respectively for both simulations.

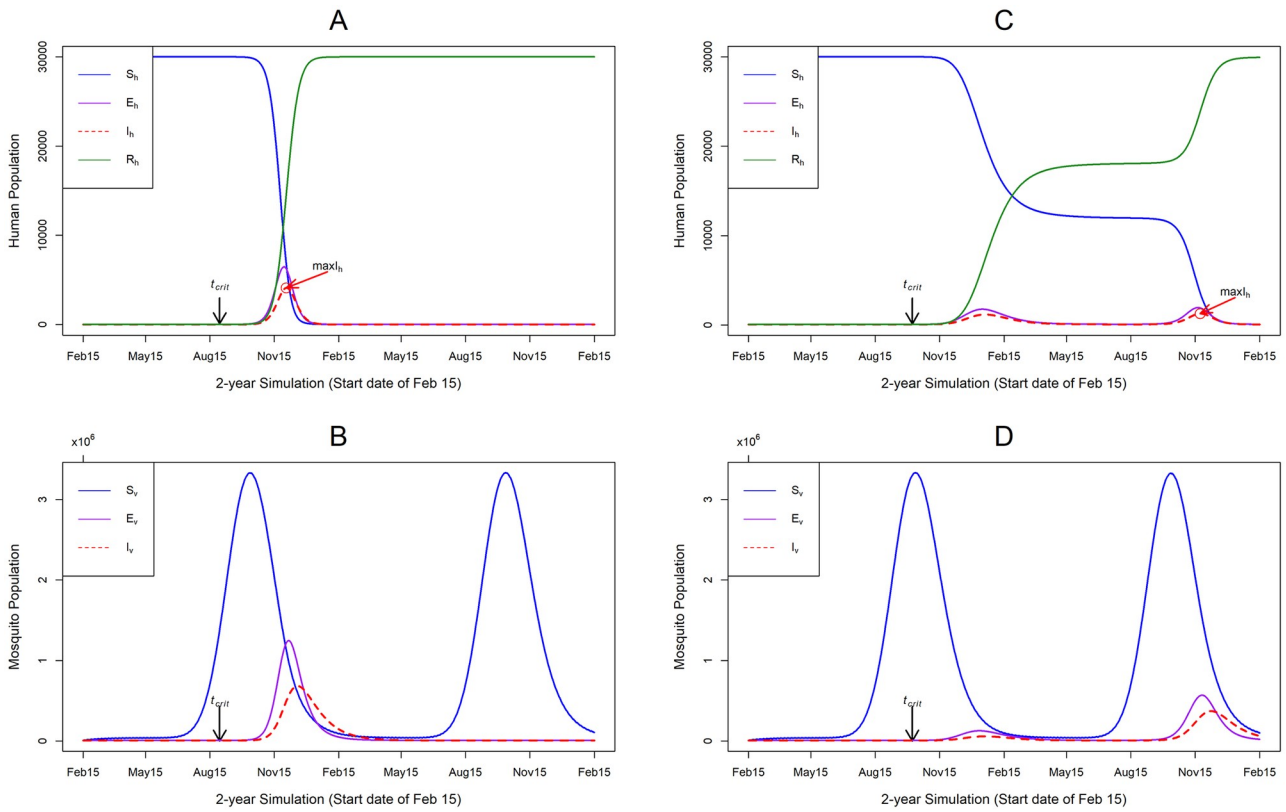

Fig 2. The epidemic progression in the human and mosquito populations. The y-axis is the number of humans or mosquitoes in the simulation and the x-axis is the 2-year simulation dates with a start date of February 15. t_{crit} = arrival date of infectious human; $maxI_h$ = the epidemic peak size, the maximum human infected at any given point during the simulation. (A) indicates the disease progression in the human population, for an arrival date of an infectious human on August 29. (C) indicates disease progression for an arrival date of an infectious human on October 7. (B) and (D) show the disease progression in the mosquito population for the respective dates of arrival. (A) shows a classical rapid epidemic, with a unimodal response, with the peak occurring few weeks after virus introduction; while (C) shows a prolonged period of lower-level transmission, resulting in a bimodal response. Default parameters from Table 2 were used for these simulations, except for dates of arrival of infectious human.

https://doi.org/10.1371/journal.pntd.0008679.g002

These results show that under the conditions used here, an epidemic potential exists within the summer and autumn seasons, with the most favorable season for a rapid outbreak being the end of the summer season. Epidemics occurring within this favorable period had an average epidemic peak size of 11% of the susceptible population infected, with a time to peak of 95 days. Arrival dates of an infectious human, in the autumn season, can dramatically affect the length of the epidemic, as these outbreaks are also modulated by the mosquito seasonal dynamics.

Seasonal variance and epidemic dynamics

To examine the epidemic dynamics as a function of the seasonal temperature variance, we simulated two different sets of temperature regimes, with a fixed arrival date in mid-summer (August 15). In the first set of temperature regimes (historical; T_{mean} varied from 19.0˚C to 22.0˚C and T_{range} varied from 4.0˚C to 6.0˚C, both in increments of 0.2˚C), all simulations resulted in an epidemic, with a classical unimodal peak. The timing and magnitude of the epidemic peak both responded differently as a function of starting temperature (calculated for August 15 from T_{mean} and T_{range} using Eq 16) with time to peak being less sensitive. Epidemic peak size increases monotonically with an increase in starting temperature, i.e. warmer

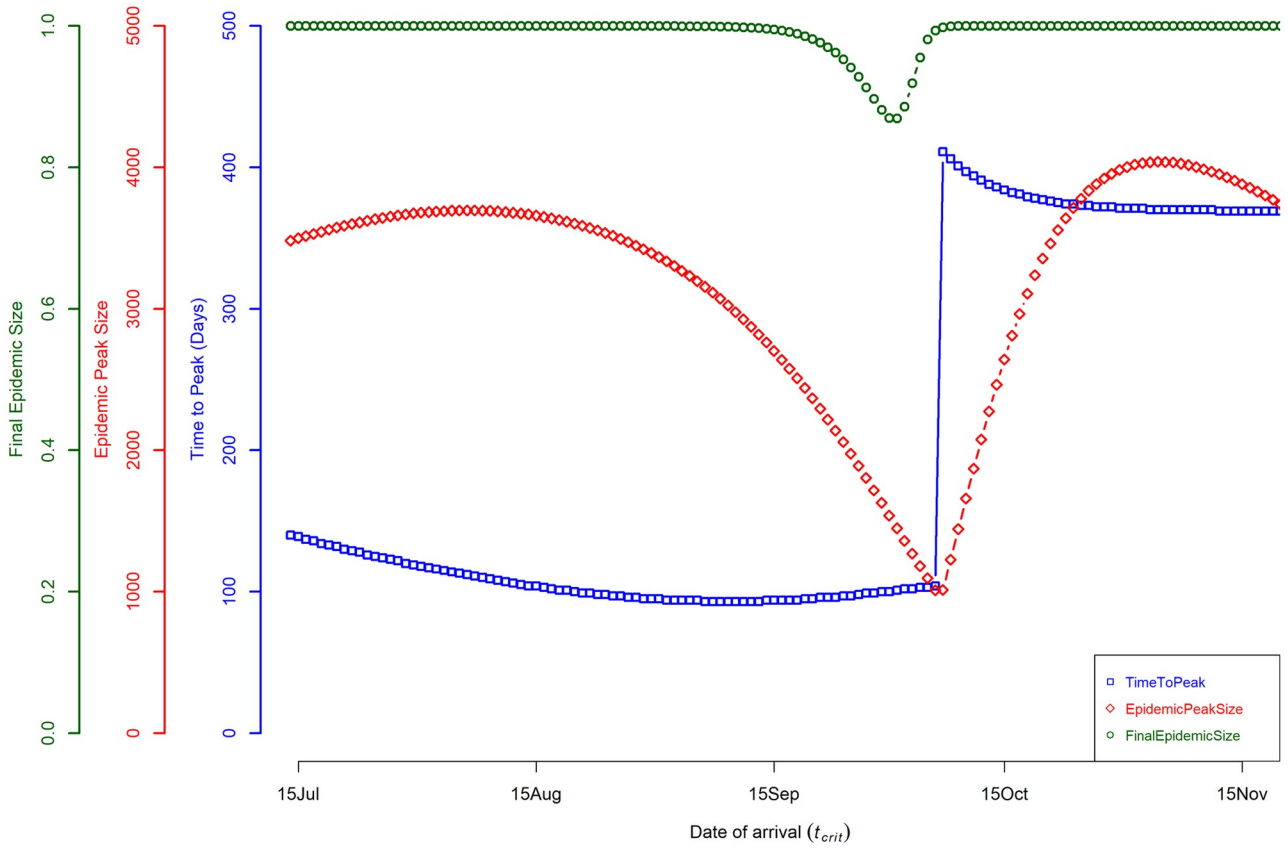

Fig 3. Quantities of interest (QOI) as a function of arrival date. QOI vs date of arrival that resulted in an epidemic by calendar date. The x-axis is the date of arrival of an infectious human, the simulation start date of February 15. The blue square points represent the time to peak infection in humans (in days). The red diamond points represent the maximum number of humans infected at any given point during the simulation. The green circle points represent the final (or cumulative) epidemic size at the end of the simulation; this is represented as the proportion of humans infected (rather than number). Simulations for arrivals dates in July to September had a classical unimodal peak, while other dates resulted in a prolonged low-level transmission, with bimodal peaks.

https://doi.org/10.1371/journal.pntd.0008679.g003

temperatures at onset produce larger epidemics within a shorter peak time and vice versa (Fig 4A). The final epidemic size was insensitive to starting temperatures, as all simulations within this regime produced final epidemic sizes of 100% of the population infected.

In the second set of temperature regimes (future; T_{mean} varied from 15.0˚C to 30.0˚C and T_{range} varied from 0.0˚C to 15.0˚C, both in increments of 0.2˚C), epidemic peak time and size show similar inverse variation as a function of starting temperature, although the overall behavior is different. Epidemic peak size had a unimodal distribution with its peak at ~28 ˚C and steadily declines afterward. Conversely the time to peak starts to increase at ~17 ˚C to ~19 ˚C, then steadily decreases until ~28 ˚C. At this peak of ~28 ˚C, the epidemic peak size was at 19% of the susceptible population infected, within a short peak time of 73 days. On the other hand, the final epidemic size steeply increases as a function of starting temperature, and plateaus at ~21 ˚C to ~30 ˚C (with 100% of the population infected), before steeply declining (Fig 4B). Extending the temperature regimes demonstrates the nonlinear influence of the interaction between mean temperature and seasonal variance on the epidemic dynamics.

To further examine this, Fig 5 shows the variation in the final epidemic size across the annual temperature bands. At a low mean annual temperature of 15˚C to 17˚C and range of 0˚C to ~7.5˚C, no epidemic occurred; however, this temperature band becomes suitable for

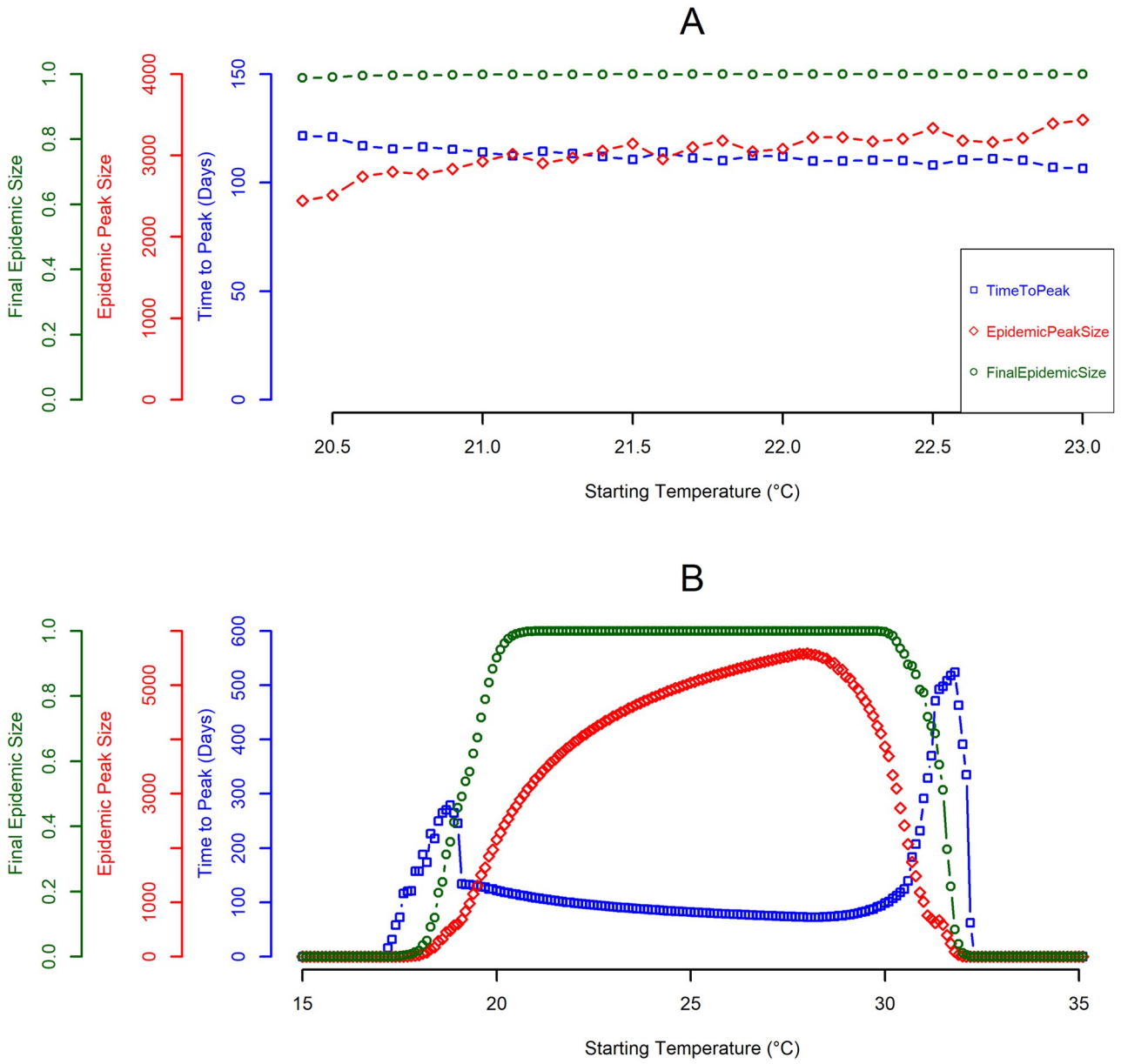

Fig 4. Quantities of interest (QOI) as a function of starting temperature. The x-axis is the starting temperatures within each set of temperature regimes and the y-axis is the associated value of the QOI being considered. Starting temperature is the temperature on August 15 calculated from T_{mean} and T_{range}. The blue square points represent the time to peak infection in humans (in days). The red diamond points represent the maximum number of humans infected at any given point during the simulation. The green circle points represent represents the final (or cumulative) epidemic size at the end of the simulation; this is represented as the proportion of humans infected (rather than number). (A) represents the historical temperature regimes, given by T_{mean} varied from 19˚C to 22˚C and T_{range} varied from 4˚C to 6˚C (both in increments of 0.2˚C), a total of 121 simulations. (B) represents the second set of temperature regimes, given by T_{mean} varied from 15˚C to 30˚C and T_{range} varied from 0˚C to 15.0˚C, a total of 5776 simulations. Due to the fixed starting date, multiple combinations of T_{mean} and T_{range} had the same starting temperature. As no other parameters were varied in these simulation sets, QOI and model behavior was identical for simulations with the same starting temperatures and overlapping points are not visible on the graphs. The default parameters from Table 2 were used for these simulations.

https://doi.org/10.1371/journal.pntd.0008679.g004

transmission as the temperature range increases beyond this point. Mean annual temperature of ~18˚C to ~26˚C, supports epidemic transmission at both low and high-temperature ranges. Epidemics introduced within these temperature regimes had the highest epidemic suitability (using final epidemic size as a measure of epidemic suitability). Lastly, mean annual

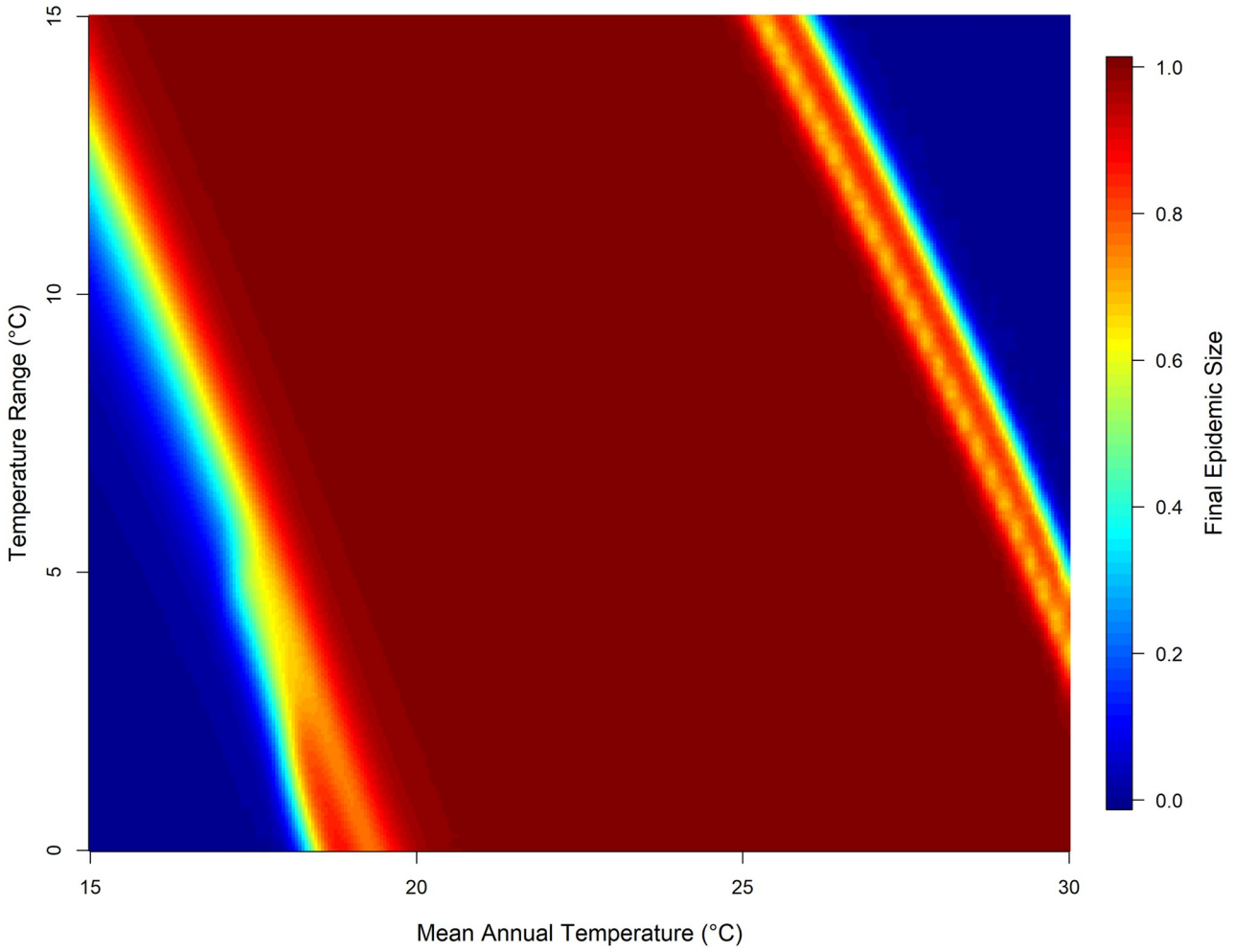

Fig 5. Final epidemic size across different seasonal temperature regimes. Heat map of final epidemic size (represented as the proportion of humans infected rather than number) as a function of mean annual temperature and temperature range. Temperature regimes here is given by T_{mean} varied from 15˚C to 30˚C and T_{range} varied from 0˚C to 15˚C, a total of 5776 simulations. Default parameters from Table 2 were used for these simulations, except for temperature parameters.

https://doi.org/10.1371/journal.pntd.0008679.g005

temperature bands of ~27˚C to 30˚C and low range of 0˚C to ~5.0˚C, transmission was supported with high epidemic suitability, this steadily diminishes as temperature range increases. In general, under the conditions used here, the dynamics of the epidemic are largely driven by the seasonal variation in temperature.

Model sensitivity analysis

Model sensitivity was characterized using 500 simulations runs for dengue parameter ranges as given in Table 2. All parameters were uniformly distributed for the LHS sampling. The conditions here were permissive for epidemics, with ($I_h > 2$) in 256 of the 500 simulated parameter sets. The epidemic progression in these parameter sets was consistent with the general model behavior seen in Fig 2A and 2C (i.e. a combination of unimodal and bimodal responses). The distribution of the QOI had a wider range of values (i.e. $MaxI_h$ = 3 to 7595 humans infected; $tmaxI_h$ = 31 to 512 days from t_{crit}; $cumI_h$ = 0.01% to 100% of the population infected), thus providing adequate variation for the sensitivity analysis.

Table 3. Sensitivity analysis of the model's quantities of interest (QOI).

Parameter	$MaxI_h$		$tmaxI_h$		$cumI_h$	
	Coefficient	Relative Importance	Coefficient	Relative Importance	Coefficient	Relative Importance
t_{crit}	0.40	**1.00**	0.43	**1.00**	0.38	**1.00**
T_{mean}	0.51	**1.00**	0.14	**1.00**	0.16	**1.00**
T_{range}	-0.20	**1.00**	-0.02	0.45	-0.13	**1.00**
$\beta_{h\rightarrow v}$	0.53	**1.00**	0.08	**1.00**	0.23	**1.00**
$\beta_{v\rightarrow h}$	0.32	**1.00**	-0.02	0.46	0.13	**1.00**
μ_v	-0.65	**1.00**	-0.05	0.85	-0.24	**1.00**
γ_v	0.05	0.38	0.00	0.25	0.01	0.33
iv	0.01	0.28	-0.01	0.35	0.00	0.27
q	0.01	0.27	0.01	0.38	0.00	0.27
R_{tot}	0.43	**1.00**	0.02	0.49	0.13	**1.00**

Relative importance and model-averaged parameter coefficient from best-supported models (confidence set of models, see S2 File for details). QOI are denoted by: $maxI_h$ = the epidemic peak size; $tmaxI_h$ = time to peak; $cumI_h$ = final epidemic size. Before model fitting, parameters were centered on zero and scaled to unit variance, to normalize parameters within the same range, hence coefficient estimates are within a range of 0.0 to 1.0; likewise the relative importance of parameters is on a scale between 0.00 and 1.00. The model-averaged coefficients effects are summarized by their direction (+|−), positive indicates the QOI increases as the parameter increases, while negative indicates QOI decreases as the parameter increases. Relative importance $\geq$0.90 appears in bold, an arbitrary cut-off for visualizing most important parameters. Notations and descriptions of parameters are denoted in Table 2.

https://doi.org/10.1371/journal.pntd.0008679.t003

Table 3 shows the relative importance of the input parameters to our QOI, using uniform LHS distributions for dengue parameters (Table 2). Considering the main effects only, our QOI were all sensitive to the arrival date of the infectious human and mean annual temperature. Epidemic size (i.e. peak and final) were both sensitive to temperature range, while time to peak was less sensitive. Other influential parameters on all the QOI were transmission rates, mortality rate, and mosquito recruitment. The time to epidemic peak was less sensitive to the mosquito life-history trait parameters in comparison to other QOI (Table 3).

All the QIO were sensitive to the interaction term between the arrival date of an infectious human and mean annual temperature and the interaction term between mean annual temperature and temperature range. Another interactive term that was influential to all QOI is the interaction between mean annual temperature and mosquito recruitment. Interactions between transmission rates and other parameters had high relative importance for time to peak, indicating that transmission rates may alter the effect of other parameters (see S2 File, S7 Table for full details).

Discussion

We extend a previous model for arbovirus transmission with multiple vectors [26] to a deterministic compartmental model for dengue fever in *Aedes aegypti* in Madeira Island. This SEI-SEIR model explores dengue epidemic dynamics as triggered by the arrival of an infected person in Funchal, Madeira, and the effects of seasonally varying temperature on transmission. Our analysis focused on three quantities of interest: time to epidemic peak, epidemic peak size, and the final size of the epidemic. We then used a global sensitivity analysis to determine which input parameters were most important to quantities of interest.

Our model demonstrates that the date of arrival of an infected human in the susceptible human population dramatically affects the overall epidemic dynamics. Arrivals in mid-summer (July) to early-autumn (September) produce epidemics more quickly after introduction with a resulting large final epidemic size. These transient epidemics are indicative of a higher

transmission potential at this point of the year and are consistent with the scenario of the 2012 outbreak [6]. Our results are also consistent with the conclusions of [8], regarding the time point in the year with the highest epidemic risk and when local control strategies should be intensified. The overall model behavior in response to the timing of virus introduction within the susceptible population is similar to other previous dengue models [27, 57].

Furthermore, our results show the interaction between seasonal temperature mean and temperature range on the epidemic dynamics. The historical temperature seasonality for Funchal, Madeira, demonstrated a highly suitable thermal environment for the vectorial capacity of *Aedes aegypti* mosquitoes and arbovirus transmission. As expected, given a favorable day of introduction, all our model simulations for this temperature regime evolved into an epidemic, with warmer temperatures at onset producing high prevalence and faster peaks. Our subsequent extension of the temperature regimes demonstrates the nonlinear influence of temperature seasonality on the epidemic dynamics. Likewise, it allowed us to examine plausible future forcing scenarios based on near-term projections of seasonal temperature changes. Overall, the thermal responses from both temperature regimes were similar to those discussed in the works of [17] and [18], which investigated the effects of temperature on dengue transmission.

Our sensitivity analysis further characterizes the variability of the epidemic dynamics to other parameters in our model. Beyond the arrival date of an infected human and temperature seasonality, the quantities of interest were also sensitive to transmission rates, mosquito mortality rate, and mosquito population size. This is consistent with other modeling studies that highlight the importance of the mosquito dynamics on epidemic outcomes [28, 58, 59]. Our sensitivity analysis went a step further to characterize the interaction effects of our model parameters. An example is the interaction term between mean temperature and the mosquito population size as demonstrated in other previous models (e.g. [13, 19, 60]). Though this was not the focus of our analysis, it can be useful in improving understanding of the complex processes that interact to determine epidemic dynamics. Likewise, from a control and mitigation perspective, the interaction term effects are useful to understand how the implementation of a specific control strategy can have dramatic effects on the mosquito life-history traits and in turn the overall epidemic dynamics. A cautionary note, our sensitivity analysis varied only the mosquito portion of the transmission cycle and does not account for the variance in the human transmission and its combined influence on the epidemic dynamics.

Putting this all together, our model is a useful mathematical tool to study different epidemic scenarios and shifts in epidemic suitability for other regions on the island, other than the south coast region, where Funchal is located. The model temperature seasonality was parameterized using the observed temperature of Funchal; however, the results can be extrapolated to other regions on the island. The near term projection (i.e. for 2016–2035) for seasonal temperature variation for the region of Madeira island (i.e. the North Atlantic, Europe, and Mediterranean region), predicts a warming of ~2˚C in annual mean temperature, with summer months of June, July and August (JJA) temperatures warming up to ~2.9˚C [46, 51]. Given our results, we can speculate that the north coast and inland regions of the island, where current annual mean temperatures suggests limited or no epidemic suitability (e.g. Santana, a municipality in the north region with annual temperatures of 16.7˚C) could have an increased potential to support transmission in the near future. The south coast region would continue to support transmission, with possible higher epidemic suitability. To reiterate, most of the simulated temperatures are very unlikely to occur on the island, except for sporadic extreme summer temperatures and heatwaves. Such sporadic extreme events have been documented, with recent abrupt changes in temperatures on the island [52, 53]. Hence our simulations provide an estimate of epidemic suitability in the likelihood of these extreme temperature conditions. Also, our results can be applicable to other islands, within the Macaronesia ecoregion with

similar climatic conditions as Madeira. For example, the island of Santiago, located in the archipelago of Cape Verde, with similar *Aedes aegypti* populations. Our results can provide insights into epidemic suitability shifts and a potential outbreak of dengue on this island. It is important to note that in real life, these projected shifts in epidemic suitability will also be influenced by other factors like rainfall, humidity, and anthropogenic activities. Thus, seasonal temperature variation must be considered jointly with these factors.

Our model did not explicitly address the scenario of multiple serotypes of dengue co-circulating in the population, and the possibility of prior exposure leading to immune interactions and increased risk of severe disease (a possibility for Funchal, given the circulating serotype for the 2012 outbreak was DENV I). However, we made the following assumption when setting the constants for the human components of the transmission cycle. We consider that infection by a serotype produces permanent immunity to it, and temporal immunity to other serotypes [42, 61, 62]. Thus, we assumed that individuals infected from the 2012 outbreak, while they have permanent immunity to the DENV-1 serotype they remain susceptible to other serotypes. Hence the constants for the intrinsic incubation and infectious periods were set to reflect an introduction of a different serotype other than DENV-1. These constants reflect mean values for DENV-2 and DENV-4 as reported in previous literature [39–43]. The analysis presented here is relevant for the introduction of a new serotype on the island, which is timely in the light of the work of [22]. Their study had demonstrated the ability of the *Aedes aegypti* populations from Madeira to transmit DENV-2, and the potential risk for the local transmission if introduced to Madeira. Our results suggest that the epidemic dynamics would be significantly impacted by the introduction of a different serotype. This emphasizes the crucial need for the island to intensify its control measures to prevent local transmission while preparing effective mitigation strategies in the event of another outbreak.

In summary, the model presented here is relevant for the introduction of a new dengue serotype into Funchal, Madeira Island, and the interaction between mean temperature and seasonal variation to drive the epidemic dynamics. Our results demonstrate the potential for summer and autumn season transmission of dengue, with varying levels of epidemic suitability, following an introduction of the virus. Overall, we demonstrated that epidemic dynamics are strongly influenced by variation in the date of arrival, seasonal temperature, transmission rates, mortality rate, and the mosquito population. The model sensitivity analysis provides insight into the relative importance of these parameters and their interactive effects as mechanistic drivers of an epidemic. These results can be a useful guide in the development of effective local control and mitigation strategies for dengue fever in Madeira Island.

Supporting information

S1 Fig. Location of Madeira Island. Map of Europe in light blue, Portugal and Azorean islands in dark blue, Madeira island circled in red.
(TIF)

S2 Fig. Location of Ovitraps in Madeira Island. The distribution of ovitrap location across the island, as reported in the Entomological panel bulletins (PEnt_RAMW52/2019, in Portuguese) of the Institute of Health Administration, IP-RAM (IASAÚDE IP-RAM). The colored dots on the map, represents the cumulative number of eggs in each location for the week 10, 2018 to week 52, 2019. Blue = 0%, Dark green = 1%-10%, Light green = 11%–20%, Yellow = 21%–30%, Orange = 31%–40%, Red = 41%–100%. Cumulative number of eggs for all location = 37766. Adapted from Institute of Health Administration, IP-RAM [34].
(TIF)

S3 Fig. Cumulative results of Ovitraps in Madeira Island. Annual cumulative number of eggs reported across the island from all the ovitraps, as reported in the Entomological panel bulletins (PEnt_RAMW52/2019, in Portuguese) of the Institute of Health Administration, IP-RAM (IASAÚDE IP-RAM). Entomological year starts from week 10. Graphs shows cumulative number of eggs for week 10, 2012 to week 52, 2019, with each entomological year represented in a different line color. Adapted from Institute of Health Administration, IP-RAM [34].
(TIF)

S4 Fig. Location of BG-traps in Madeira Island. The distribution of BG-traps location across the island, as reported in the Entomological panel bulletins (PEnt_RAMW52/2019, in Portuguese) of the Institute of Health Administration, IP-RAM (IASAÚDE IP-RAM). The colored dots on the map, represents the cumulative number of adult mosquitoes in each location for the week 10, 2018 to week 52, 2019. Blue = 0%, Dark green = 1%-10%, Light green = 11%–30%, Yellow = 31%–50%, Orange = 51%–60%, Red = 61%–100%. Cumulative number of adult mosquitoes for all location = 3464. Adapted from Institute of Health Administration, IP-RAM [34].
(TIF)

S5 Fig. Cumulative results of BG-traps in Madeira Island. Annual cumulative number of adult mosquitos reported across the island from all the BG-traps, as reported in the Entomological panel bulletins (PEnt_RAMW52/2019, in Portuguese) of the Institute of Health Administration, IP-RAM (IASAÚDE IP-RAM). Entomological year starts from week 10. Graphs shows cumulative number of eggs for week 40, 2012 to week 52, 2019, with each entomological year represented in a different line color. Adapted from Institute of Health Administration, IP-RAM [34].
(TIF)

S6 Fig. Seasonal temperature pattern. The temperature seasonality pattern as observed from the historical decadal data for Funchal, Madeira. Average of minimum (green line), mean (blue line) and maximum (red line) temperatures per day between 2008 and 2018. Black dashed line is daily mean temperature of our model as calculated from sinusoidal curve (Eq 16 in the main article). The long-term average conditions in Funchal, Madeira T_{max} = 22˚C, T_{mean} = 20˚C, T_{min} = 17˚C. Average mean temperatures for the spring months (Mar–May) was 18˚C; Summer months (Jun–Aug) was 22˚C; Autumn months (Sep–Nov) was 21˚C and Winter months (Dec–Feb) was 17˚C.
(TIF)

S1 File. S1 Appendix. Model starting conditions.
(DOCX)

S2 File. S2 Appendix. Model sensitivity analysis and multi-model inference analysis.
(DOCX)

Acknowledgments

We appreciate Joe Pohedra who assisted in the programming of the initial transmission model and Jebidiah Light who assisted with the adaption to the current SEI-SEIR model.

Author Contributions

Conceptualization: Donald Salami, César Capinha, Carla Alexandra Sousa, Maria do Rosário Oliveira Martins, Cynthia Lord.

Formal analysis: Donald Salami.

Methodology: Donald Salami, Cynthia Lord.

Software: Cynthia Lord.

Supervision: César Capinha, Carla Alexandra Sousa, Maria do Rosário Oliveira Martins, Cynthia Lord.

Visualization: Donald Salami.

Writing – original draft: Donald Salami.

Writing – review & editing: Donald Salami, César Capinha, Carla Alexandra Sousa, Maria do Rosário Oliveira Martins, Cynthia Lord.

References

1. Messina JP, Brady OJ, Golding N, Kraemer MUG, Wint GRW, Ray SE, et al. The current and future global distribution and population at risk of dengue. Nat Microbiol. 2019. https://doi.org/10.1038/s41564-019-0476-8.
2. Kraemer MUG, Hay SI, Pigott DM, Smith DL, Wint GRW, Golding N. Progress and challenges in infectious disease cartography. Trends Parasitol. 2016; 32(1):19–29. https://doi.org/10.1016/j.pt.2015.09.006. PMID: 26604163
3. Leta S, Beyene TJ, De Clercq EM, Amenu K, Kraemer MUG, Revie CW. Global risk mapping for major diseases transmitted by *Aedes aegypti and Aedes albopictus*. Int J Infect Dis. 2018; 67:25–35. https://doi.org/10.1016/j.ijid.2017.11.026. PMID: 29196275
4. Margarita Y, Grácio AS, Lencastre I, Silva A, Novo T, Sousa C. First record of *Aedes* (*stegomyia*) *aegypti* (Linnaeus, 1762) (Diptera, culicidae) in Madeira Island—Portugal (in portguese) Acta Parasitol Port. 2006; 13:59–61.
5. Medlock JM, Hansford KM, Schaffner F, Versteirt V, Hendrickx G, Zeller H, et al. A review of the invasive mosquitoes in Europe: ecology, public health risks, and control options. Vector Borne Zoonotic Dis. 2012; 12(6):435–47. https://doi.org/10.1089/vbz.2011.0814. PMID: 22448724
6. ECDC. Dengue outbreak in madeira (2012–13) 2013. European Centre for Disease Prevention and Control [17 Jul 2019]. https://ecdc.europa.eu/en/dengue-fever/threats-and-outbreaks/madeira-outbreak-2012.
7. ECDC. Update on autochthonous dengue cases in Madeira, Portugal. Stockholm: European Centre for Disease Prevention and Control, 2012. https://ecdc.europa.eu/sites/portal/files/media/en/publications/Publications/dengue-madeira-risk-assessment-update.pdf.
8. Lourenco J, Recker M. The 2012 Madeira dengue outbreak: epidemiological determinants and future epidemic potential. PLoS Negl Trop Dis. 2014; 8(8):e3083. https://doi.org/10.1371/journal.pntd.0003083. PMID: 25144749
9. Watts DM, Burke DS, Harrison BA, Whitmire RE, Nisalak A. Effect of temperature on the vector efficiency of *Aedes aegypti* for dengue 2 virus. Am J Trop Med Hyg.1987; 36(1):143–52. https://doi.org/10.4269/ajtmh.1987.36.143. PMID: 3812879
10. Rueda LM, Patel KJ, Axtell RC, Stinner RE. Temperature-dependent development and survival rates of *Culex quinquefasciatus* and *Aedes aegypti* (Diptera: Culicidae). J Med Entomol. 1990; 27(5):892–8. https://doi.org/10.1093/jmedent/27.5.892 PMID: 2231624
11. Eisen L, Monaghan AJ, Lozano-Fuentes S, Steinhoff DF, Hayden MH, Bieringer PE. The impact of temperature on the bionomics of *Aedes* (*stegomyia*) aegypti, with special reference to the cool geographic range margins. J Med Entomol. 2014; 51(3):496–516. https://doi.org/10.1603/ME13214 PMID: 24897844
12. Couret J, Dotson E, Benedict MQ. Temperature, larval diet, and density effects on development rate and survival of *Aedes aegypti* (Diptera: Culicidae). PloS One. 2014; 9(2):e87468. https://doi.org/10.1371/journal.pone.0087468. PMID: 24498328

13. Yang HM, Macoris ML, Galvani KC, Andrighetti MT, Wanderley DM. Assessing the effects of temperature on the population of *Aedes aegypti*, the vector of dengue. Epidemiol Infect. 2009; 137(8):1188–202. https://doi.org/10.1017/s0950268809002040. PMID: 19192322

14. Johansson MA, Powers AM, Pesik N, Cohen NJ, Staples JE. Nowcasting the spread of chikungunya virus in the Americas. PloS One. 2014; 9(8):e104915. https://doi.org/10.1371/journal.pone.0104915. PMID: 25111394

15. Liu-Helmersson J, Stenlund H, Wilder-Smith A, Rocklöv J. Vectorial capacity of *Aedes aegypti*: effects of temperature and implications for global dengue epidemic potential. PloS One. 2014; 9(3):e89783. https://doi.org/10.1371/journal.pone.0089783. PMID: 24603439

16. Morin CW, Monaghan AJ, Hayden MH, Barrera R, Ernst K. Meteorologically driven simulations of dengue epidemics in San Juan, PR. PLoS Negl Trop Dis. 2015; 9(8):e0004002. https://doi.org/10.1371/journal.pntd.0004002. PMID: 26275146

17. Mordecai EA, Cohen JM, Evans MV, Gudapati P, Johnson LR, Lippi CA, et al. Detecting the impact of temperature on transmission of zika, dengue, and chikungunya using mechanistic models. PLoS Negl Trop Dis. 2017; 11(4):e0005568. https://doi.org/10.1371/journal.pntd.0005568. PMID: 28448507

18. Huber JH, Childs ML, Caldwell JM, Mordecai EA. Seasonal temperature variation influences climate suitability for dengue, chikungunya, and zika transmission. PLoS Negl Trop Dis. 2018; 12(5):e0006451. https://doi.org/10.1371/journal.pntd.0006451. PMID: 29746468

19. Mordecai EA, Caldwell JM, Grossman MK, Lippi CA, Johnson LR, Neira M, et al. Thermal biology of mosquito-borne disease. Ecol Lett. 2019; 0(0). https://doi.org/10.1111/ele.13335.

20. Fernandopullé D. Climatic characteristics of the Canary Islands. In: K G., editor. Biogeography and ecology in the Canary Islands: Springer, Dordrecht; 1976. p. 185–206.

21. Santos FD, Valente MA, Miranda PMA, Aguiar A, Azevedo EB, Tomé AR, et al. Climate change scenarios in the Azores and Madeira Islands. World Resour Rev. 2004; 16(4):473–91. http://idlcc.fc.ul.pt/pdf/SantosEtalWRR2004.pdf.

22. Seixas G, Jupille H, Yen P-S, Viveiros B, Failloux A-B, Sousa CA. Potential of *Aedes aegypti* populations in Madeira Island to transmit dengue and chikungunya viruses. Parasit Vectors. 2018; 11(1):509. https://doi.org/10.1186/s13071-018-3081-4. PMID: 30208974

23. Messina JP, Brady OJ, Pigott DM, Brownstein JS, Hoen AG, Hay SI. A global compendium of human dengue virus occurrence. Sci Data. 2014; 1:140004. https://doi.org/10.1038/sdata.2014.4. PMID: 25977762

24. Guo C, Zhou Z, Wen Z, Liu Y, Zeng C, Xiao D, et al. Global epidemiology of dengue outbreaks in 1990–2015: A systematic review and meta-analysis. Front Cell Infect Microbiol. 2017; 7:317-. https://doi.org/10.3389/fcimb.2017.00317. PMID: 28748176

25. Ryan SJ, Carlson CJ, Mordecai EA, Johnson LR. Global expansion and redistribution of Aedes-borne virus transmission risk with climate change. PLoS Negl Trop Dis. 2019; 13(3):e0007213. https://doi.org/10.1371/journal.pntd.0007213. PMID: 30921321

26. Lord CC, Lounibos LP, Pohedra JJ, Alto BW. Effects of mosquito biology on modeled chikungunya virus invasion potential in Florida. Viruses 2020, 12(8), 830; https://doi.org/10.3390/v12080830.

27. Otero M, Solari HG. Stochastic eco-epidemiological model of dengue disease transmission by Aedes aegypti mosquito. Math Biosci. 2010; 223(1):32–46. https://doi.org/10.1016/j.mbs.2009.10.005. PMID: 19861133

28. Manore CA, Hickmann KS, Xu S, Wearing HJ, Hyman JM. Comparing dengue and chikungunya emergence and endemic transmission in A. aegypti and A. albopictus. J Theor Biol. 2014; 356:174–91. https://doi.org/10.1016/j.jtbi.2014.04.033. PMID: 24801860

29. Karl S, Halder N, Kelso JK, Ritchie SA, Milne GJ. A spatial simulation model for dengue virus infection in urban areas. BMC Infect Dis. 2014; 14:447. https://doi.org/10.1186/1471-2334-14-447. PMID: 25139524

30. Ferreira CP, Godoy WAC. Ecological modelling applied to entomology. Switzerland: Springer; 2014.

31. Institute of Health Administration, IP-RAM. Mosquito on Madeira Island (in Portuguese). Institute of Health Administration, IP-RAM, Regional Secretariat of Health, Autonomous Region of Madeira; 2019 [17 Jul 2019]. http://doc.iasaude.pt/mosquito/index.php/mosquito/mosquito-na-ilha-da-madeira.

32. Duong V, Lambrechts L, Paul RE, Ly S, Lay RS, Long KC, et al. Asymptomatic humans transmit dengue virus to mosquitoes. Proc Natl Acad Sci. 2015; 112(47):14688–93. https://doi.org/10.1073/pnas.1508114112. PMID: 26553981

33. Newton EA, Reiter P. A model of the transmission of dengue fever with an evaluation of the impact of ultra-low volume (ulv) insecticide applications on dengue epidemics. The Am J Trop Med Hyg. 1992; 47(6):709–20. https://doi.org/10.4269/ajtmh.1992.47.709. PMID: 1361721

34. Menach AL, McKenzie FE, Flahault A, Smith DL. The unexpected importance of mosquito oviposition behaviour for malaria: non-productive larval habitats can be sources for malaria transmission. Malar J. 2005; 4(1):23. https://doi.org/10.1186/1475-2875-4-23.

35. Institute of Health Administration, IP-RAM. Entomological panel bulletins(in Portuguese). IASAÚDE IP-RAM, Sanitary Engineering Unit: Institute of Health Administration, IP-RAM, Regional Secretariat of Health, Autonomous Region of Madeira, 2019. http://doc.iasaude.pt/mosquito/index.php/boletins/entomologicos.

36. Scott TW, Amerasinghe PH, Morrison AC, Lorenz LH, Clark GG, Strickman D, et al. Longitudinal studies of aedes aegypti (diptera: Culicidae) in thailand and puerto rico: blood feeding frequency. J. Med. Entomol. 2000; 37(1):89–101. https://doi.org/10.1603/0022-2585-37.1.89. PMID: 15218911

37. Paupy C, Ollomo B Fau—Kamgang B, Kamgang B Fau—Moutailler S, Moutailler S Fau—Rousset D, Rousset D Fau—Demanou M, Demanou M Fau—Herve J-P, et al. Comparative role of Aedes albopictus and Aedes aegypti in the emergence of dengue and chikungunya in central Africa. Vector Borne Zoonotic Dis. 2010; 10(3). https://doi.org/10.1089/vbz.2009.0005.

38. Lord CC. The effect of multiple vectors on arbovirus transmission. Isr J Ecol Evol. 2010; 56(3–4):371–92. https://doi.org/10.1560/ijee.55.3-4.371. PMID: 23741205

39. Focks DA, Barrera R. Dengue transmission dynamics: Assessment and implications for control. CiteSeer: World health organization on behalf of the special programme for research and training in tropical diseases, 2007. http://citeseerx.ist.psu.edu/viewdoc/summary?doi=10.1.1.612.689.

40. Nishiura H, Halstead SB. Natural history of dengue virus (DENV)-1 and DENV-4 infections: reanalysis of classic studies. J Infect Dis. 2007; 195(7):1007–13. https://doi.org/10.1086/511825. PMID: 17330791

41. Chan M, Johansson MA. The incubation periods of dengue viruses. PloS One. 2012; 7(11):e50972. https://doi.org/10.1371/journal.pone.0050972. PMID: 23226436

42. Lourenco J, Recker M. Dengue serotype immune-interactions and their consequences for vaccine impact predictions. Epidemics. 2016; 16:40–8. https://doi.org/10.1016/j.epidem.2016.05.003. PMID: 27663790

43. Gubler DJ, Suharyono W, Tan R, Abidin M, Sie A. Viraemia in patients with naturally acquired dengue infection. Bull World Health Organ. 1981; 59(4):623–30. https://www.ncbi.nlm.nih.gov/pubmed/6976230.

44. Vaughn DW, Green S, Kalayanarooj S, Innis BL, Nimmannitya S, Suntayakorn S, et al. Dengue viremia titer, antibody response pattern, and virus serotype correlate with disease severity. J Infect Dis. 2000; 181(1):2–9. https://doi.org/10.1086/315215. PMID: 10608744

45. Santo António Parish Council. History of Santo António parish council (in Portuguese): junta de freguesia de Santo António- an autonomous region of Madeira; 2018 [17 Jul 2019]. http://www.jf-santoantonio.pt/historia.

46. Weather Underground. Weather history for Funchal Madeira (2008–2018) 2019 [01 Mar 2019]. https://www.wunderground.com/history/daily/pt/funchal/LPMA.

47. IPCC. Climate change 2013: The physical science basis. Contribution of working group i to the fifth assessment report of the intergovernmental panel on climate change. Cambridge University Press, Cambridge, United Kingdom, and New York, NY, USA: 2013; [1535]. https://www.ipcc.ch/report/ar5/wg1/.

48. Funchal city hall. Funchal natural history museum: Funchal city hall (Câmara Municipal do Funchal) 2019. http://www.cm-funchal.pt/pt/servi%C3%A7os/ci%C3%AAncia/museu-de-hist%C3%B3ria-natural-do-funchal/sobre-o-museu.html.

49. Andraud M, Hens N, Marais C, Beutels P. Dynamic epidemiological models for dengue transmission: a systematic review of structural approaches. PloS One. 2012; 7(11):e49085. https://doi.org/10.1371/journal.pone.0049085. PMID: 23139836

50. Kiraly A, Janosi IM. Stochastic modeling of daily temperature fluctuations. Phys Rev. 2002; 65(1539–3755 (Print)):051102 1–6. https://doi.org/10.1103/PhysRevE.65.051102.

51. Lord CC, Day JF. Simulation studies of st. Louis encephalitis virus in south Florida. Vector Borne Zoonotic Dis. 2001; 1(4):299–315. https://doi.org/10.1089/15303660160025921. PMID: 12653129

52. Seneviratne SI, Field CB, Barros V, Stocker TF, Dahe Q, Dokken DJ, et al. Managing the risks of extreme events and disasters to advance climate change adaptation. Cambridge: Intergovernmental panel on climate change 2012; [582]. https://www.ipcc.ch/report/managing-the-risks-of-extreme-events-and-disasters-to-advance-climate-change-adaptation/.

53. Madeira Island News. Madeira heatwave continues. Madeira Island News, 2016 [17 Jul 2019]. https://www.madeiraislandnews.com/2016/08/heatwave-continues.html.

54. Madeira Island News. Hottest December day for 150 years. Madeira Island News, 2018 [17 Jul 2019]. https://www.madeiraislandnews.com/2018/12/hottest-december-day-for-150-years.html.

55. MathWorks. MATLAB and Statistics Toolbox Release 2016a. Natick, Massachusetts: The MathWorks Inc.; 2016.

56. Calcagno V, de Mazancourt C. Glmulti: an R package for easy automated model selection with (generalized) linear models. 2010. 2010; 34(12): J Stat Softw. https://doi.org/10.18637/jss.v034.i12.

57. R-Core-Team. The R project for statistical computing: CRAN; 2019. https://www.r-project.org/.

58. Erickson RA, Presley SM, Allen LJS, Long KR, Cox SB. A dengue model with a dynamic Aedes albopictus vector population. Ecol Model. 2010; 221(24):2899–908. https://doi.org/10.1016/j.ecolmodel.2010.08.036.

59. Ellis AM, Garcia AJ, Focks DA, Morrison AC, Scott TW. Parameterization and sensitivity analysis of a complex simulation model for mosquito population dynamics, dengue transmission, and their control. Am J Trop Med Hyg. 2011; 85(2):257–64. https://doi.org/10.4269/ajtmh.2011.10-0516. PMID: 21813844

60. Ndii MZ, Hickson RI, Allingham D, Mercer GN. Modelling the transmission dynamics of dengue in the presence of Wolbachia. Math Biosci. 2015; 262:157–66. https://doi.org/10.1016/j.mbs.2014.12.011. PMID: 25645184

61. Yang HM, Macoris ML, Galvani KC, Andrighetti MT, Wanderley DM. Assessing the effects of temperature on dengue transmission. Epidemiol Infect. 2009; 137(8):1179–87. https://doi.org/10.1017/s0950268809002052. PMID: 19192323

62. Wearing HJ, Rohani P. Ecological and immunological determinants of dengue epidemics. Proc Natl Acad Sci. 2006; 103(31):11802–7. https://doi.org/10.1073/pnas.0602960103. PMID: 16868086